Occipital-Callosal Pathways in Children

Validation and Atlas Development

ROBERT F. DOUGHERTY,[a,b] MICHAL BEN-SHACHAR,[a,b] GAYLE DEUTSCH,[a] POLINA POTANINA,[a] ROLAND BAMMER,[c] AND BRIAN A. WANDELL[a,b,d]

[a]*Stanford Institute for Reading and Learning,* [b]*Psychology Department,* [c]*Radiology Department,* [d]*Neurosciences Program, Stanford University, Stanford, California, USA*

ABSTRACT: Diffusion tensor imaging and fiber tracking were used to measure fiber bundles connecting the two occipital lobes in 53 children of 7–12 years of age. Independent fiber bundle estimates originating from the two hemispheres converge onto the lower half of the splenium. This observation validates the basic methodology and suggests that most occipital-callosal fibers connect the two occipital lobes. Within the splenium, fiber bundles are organized in a regular pattern with respect to their cortical projection zones. Visual cortex dorsal to calcarine projects through a large band that fills much of the inferior half of the splenium, while cortex ventral to calcarine sends projections through a band at the anterior inferior edge of the splenium. Pathways projecting to the occipital pole and lateral-occipital regions overlap the dorsal and ventral groups slightly anterior to the center of the splenium. To visualize these pathways in a typical brain, we combined the data into an atlas. The estimated occipital-callosal fiber paths from the atlas form the walls of the occipital horn of the lateral ventricle, with dorsal paths forming the medial wall and the ventral paths bifurcating into a medial tract to form the inferior-medial wall and a superior tract that joins the lateral-occipital paths to form the superior wall of the ventricle. The properties of these fiber bundles match those of the hypothetical pathways described in the neurological literature on alexia.

KEYWORDS: diffusion tensor imaging; fiber tracking; splenium; alexia; white matter atlas

INTRODUCTION

The white matter fiber bundles that connect distant cortical regions are essential for neural computations, and damage to these bundles produces striking neuropsychological deficits. Proper fiber bundle development requires remarkable coordination between source and target neurons in the developing brain. Variations in the precision or stability of these long-range connections may account for important aspects of behavioral and cognitive performance.[1,2]

The magnetic resonance imaging method of diffusion tensor imaging (DTI), coupled with fiber-tracking (FT) algorithms, promises to provide substantial infor-

Address for correspondence: Robert F. Dougherty, Psychology Department, Jordan Hall, Building 420, Stanford University, Stanford, CA 94305-2130. Voice: 650-725-2466.
bobd@stanford.edu

Ann. N.Y. Acad. Sci. 1064: 98–112 (2005). © 2005 New York Academy of Sciences.
doi: 10.1196/annals.1340.017

mation about human fiber bundles and their development.[3–12] An important objective of DTI-FT methods is to clarify the specific behavioral consequences associated with fiber bundles in individual subjects. For example, DTI methods make it possible to compare an individual's behavior or skill level with white matter structure.[13,14] It is also possible to study white matter fiber bundles in individual subjects with specific behavioral disorders.[15]

A quantitative description of typical white matter is essential for understanding how deviations from the norm impact behavior. One useful description of white matter properties takes the form of a template that describes the typical DTI values and their variance in a normal population. In those portions of the white matter where fiber tracts can be reliably estimated, it is further useful to label template structures, including fiber bundles and the paths that they traverse. A number of groups are developing such atlases.[16]

Here, we describe our measurements of typical white matter properties in children. We concentrate on fiber bundles that pass through the splenium of the corpus callosum and connect the occipital lobes (occipital-callosal fiber tracts). In adults, we previously found that these fiber pathways can be estimated reliably. Here, we extend those findings to a larger population of children ($N = 53$; 7–12 years old).

Finally, we use these measurements to identify the fiber bundles likely to be involved in a specific reading deficit, pure alexia.[15,17–20] Specifically, we analyze the positions of the white matter lesions described in the literature with respect to the fiber bundles in the atlas. This analysis identifies specific long-range splenial fiber bundles that are important for fluent reading and probably for proper reading development.

METHODS

Subjects

Children were recruited from the San Francisco Bay region of California ($N = 53$; 7–12 years old). Written informed consent/assent was obtained from all children and parents. All subjects were physically healthy and had no history of neurological disease, head injury, attention deficit/hyperactivity disorder, or psychiatric disorder. The Stanford Panel on Human Subjects in Medical and Non-Medical Research approved all procedures.

The data were collected as part of a longitudinal study of reading development and represent the first measurement time point. All subjects also participated in neuropsychological testing and functional MRI scan sessions, but these data will not be discussed here.

Magnetic Resonance Imaging Protocols

MR data were acquired on 1.5T Signa LX (Signa CVi, GE Medical Systems, Milwaukee, WI) using a self-shielded, high-performance gradient system capable of providing a maximum gradient strength of 50 mT/m at a gradient rise time of 268 μs for each of the gradient axes. A standard quadrature head coil, provided by the vendor, was used for excitation and signal reception. Head motion was minimized by placing cushions around the head and securing a Velcro strap across the forehead.

Children watched and listened to cartoons via a video projection system and pneumatic headphones (Resonance Technologies, Northridge, CA) during the scan session to occupy their attention and reduce anxiety.

The DTI protocol involved 8–10 repeats of a 90-s whole-brain scan. These repeats were averaged to improve signal quality. The pulse sequence was a diffusion-weighted single-shot spin-echo, echo-planar imaging sequence (TE = 63 ms; TR = 6 s; FOV = 260 mm; matrix size = 128 × 128; bandwidth = ±110 kHz; partial *k*-space acquisition). We acquired 48–54 axial, 2-mm-thick slices (no skip) for two *b*-values: $b = 0$ and $b = \sim 800$ s/mm^2. The high *b*-value was obtained by applying gradients along 12 different diffusion directions. Two gradient axes were energized simultaneously to minimize TE: G0 = $(0\ 0\ 0)^T$, G1 = $1/\sqrt{2}\ (1\ 1\ 0)^T$, G2 = $1/\sqrt{2}\ (1\ 0\ 1)^T$, G3 = $1/\sqrt{2}\ (0\ 1\ 1)$, G4 = $1/\sqrt{2}\ (-1\ 1\ 0)^T$, G5 = $1/\sqrt{2}\ (-1\ 0\ 1)^T$, and G6 = $1/\sqrt{2}\ (0\ -1\ 1)$. This pattern was repeated twice for each slice. The polarity of the effective diffusion-weighting gradients was reversed for odd repetitions to remove cross-terms between diffusion gradients and both imaging and background gradients.

DTI data were preprocessed using a custom program based on normalized mutual information that removed eddy current distortion effects and determined a constrained nonrigid image registration.[21] The six elements of the diffusion tensor were determined by multivariate regression using matrix calculations on a per voxel basis.[22–24]

We also collected high-resolution T1-weighted anatomical images using a 3D-SPGR sequence (~1 × 1 × 1 mm voxel size). We routinely collected 3–4 3D-SPGR scans (both axial and sagittal slice orientations) and coregistered and averaged all scans that were relatively artifact-free.

Fiber-Tracking Algorithms and Software

For each subject, the T2-weighted ($b = 0$) images were aligned to the T1-weighted 3D-SPGR anatomical images. The alignment was initiated using the scanner coordinates stored in the image headers. This alignment was refined using a mutual-information 3D rigid-body algorithm from SPM2.[25] Several anatomical landmarks, including the anterior commissure (AC), the posterior commissure (PC), and another point in the midsagittal plane, were identified by hand in the T1 images. With these landmarks, we computed a rigid-body transform from the native image space to the conventional AC–PC aligned space, with the AC at the origin, the AC–PC line forming the y-axis, the AC–midsagittal line forming the z-axis, and the remaining orthogonal (left–right) forming the x-axis. The DTI data were then resampled to this AC–PC aligned space with 2-mm isotropic voxels using a spline-based tensor interpolation algorithm,[26] taking care to rotate the tensors to preserve their orientation with respect to the anatomy.[27] The T1 images were resampled to AC–PC aligned space with 1-mm isotropic voxels. We confirmed that this coregistration technique aligns the DTI and T1 images to within 1–2 mm in the occipital lobes. However, the well-known geometric distortions inherent in EPI acquisition limit the accuracy in regions prone to susceptibility artifacts, such as orbitofrontal and anterior temporal regions.

Fiber bundles were estimated using a streamlines tracking algorithm[3,6,10] with a fourth-order Runge-Kutta path integration method[28] and 1-mm fixed step size. A continuous tensor field was estimated using trilinear interpolation of the tensor elements. Path tracing proceeded until the FA fell below 0.15, or until the minimum

angle between the current and previous path segments was larger than 30°. Both directions from the initial seed point principal diffusion axis were traced.

The seed points were laid down in a grid that filled the white matter of the left or right occipital lobe (defined in each subject by hand) at 1-mm spacing. About 16,000 estimated fiber paths were identified in each hemisphere. As we focused on callosal projections for these analyses, only fiber bundles that passed through the corpus callosum were retained. This was typically about 20% of the total left or right fibers.

Creating Average Tensor Maps

To facilitate individual subject analyses and allow averaging of the diffusion tensor field across subjects, we computed a smooth deformation of each subject's brain to a custom brain template. This deformation was used in the dorsal/ventral/lateral segmentation analysis to warp regions of interest (defined on the cortical surface of one subject) to all subjects. These deformations were also used to create an average tensor map for visualizing the expected path of the occipital-callosal fibers.

The deformation was computed based on the high-resolution T1-weighted images. A brain mask was computed for each of these using the brain extraction tool (BET, version 2.1) from the Oxford FMRIB Analysis Group.[29] By stripping the skull with this brain mask, we avoid the false-matches between brain-edge and scalp-edge that occasionally occur when the skull and scalp are included in the images.

The final template and average tensor map was created by an iterative process. An initial T1-weighted template was created by resampling each brain to a common space (similar to that of Talairach and Tournoux) based on landmarks that were defined by hand in each subject, and then averaging all the resampled, skull-stripped, brains. This avoids the biases inherent in basing the final template on a single subject or on a template comprising a different sample. This method also ensures that the final template is representative of the group in shape and size. As described above, the T1-weighted images were initially transformed with a rotation and translation into AC–PC space, with 1-mm isotropic voxels. To further align the brains for creating the initial atlas, we also marked six points in each brain that defined the maximal extent of the cortical surface along each of the three axes. These six landmarks were used to define seven different scale factors: two along the x-axis (left of the AC and right of the AC), two along the z-axis (inferior of the AC and superior of the AC), and three along the y-axis (anterior of the AC, posterior of the PC, and the AC-to-PC section were all scaled separately). The scale factors were chosen so that the maximal extent of each brain would end up at the mean position of all 53 brains. The mean extents for the 53 brains were 71.8 mm for superior of AC, 40.5 mm for inferior of AC, 66.1 mm for right of AC, 66.7 mm for left of AC, 68.0 mm for anterior of AC, 25.1 mm for AC-to-PC, and 75.4 mm for posterior of PC.

Next, an intermediate template was created by spatially normalizing the original (skull-stripped) brains to this initial template using the nonlinear deformation algorithm from SPM2.[30] These intermediate images were averaged to create a refined template, which had a more sharply defined brain-edge and ventricles. Finally, we spatially normalized the original (skull-stripped) brains (again, using the SPM2 tools) to this refined template. For each brain, this deformation—mapping the T1-weighted images to the intermediate template—was also applied to the diffusion tensor map, taking care to rotate the tensors to preserve their orientation.[31] When

applying the deformations, the T1-weighted volume was resampled to a 1-mm grid and the tensor map was resampled to a 2-mm grid, both using trilinear interpolation. Finally, all of these resampled T1-weighted images and diffusion tensor maps were then averaged to produce the mean tensor map and T1-weighted template.

These templates, along with the custom software used for all the analysis and visualization, can be obtained from the authors upon request.

RESULTS

Comparison of Right and Left Occipital-Callosal Bundle Positions

We evaluate the reliability of fiber bundle estimates by comparing estimates derived from two independent data sets. We first define two independent volumes of interest (VOI) comprising all the white matter in the left and right occipital lobes. We then compare where fibers from these two sets cross the callosum. Any occipital-occipital fiber tract has a single crossing point in the callosum. Hence, if occipital-occipital fibers are properly identified by DTI-FT applied to the left and the right, then the estimated fibers from these two data sets should meet at a common position in the callosum.

There are two reasons why a callosal location would be identified in one estimate, but not the other. First, a fiber tract may pass from the occipital lobe through the callosum and project somewhere other than the occipital lobe. Such a fiber would not have a matching counterpart from the other occipital lobe. Second, the DTI-FT algorithm may make a type I or II error. In the case of poor sensitivity, the algorithm correctly estimates the portion of the fiber tract in, say, the left occipital lobe, but fails to identify the matching portion in the right lobe. Alternatively, the estimated occipital-callosal tract may not exist.

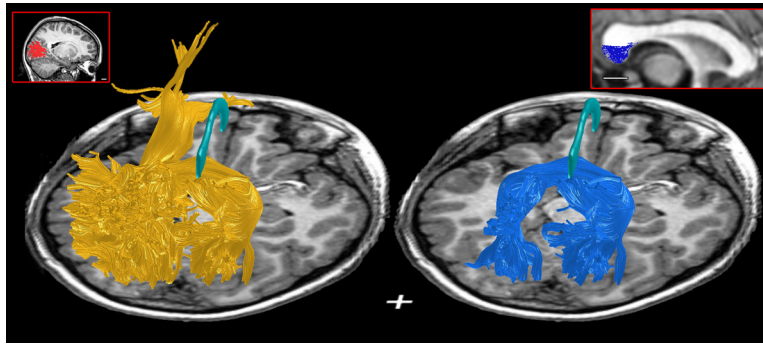

FIGURE 1. Method for estimating occipital-callosal fiber bundles. A region of interest is selected in the occipital lobe of one hemisphere (sagittal image showing red overlay; upper left inset). The points in this region of interest serve as seed locations to estimate all fiber bundles that pass through the occipital lobe (yellow fibers in the left image). The subset of occipital-lobe fibers that pass through the corpus callosum (shown in cyan) are identified (blue fiber bundles in the right image). The location of these fibers in the plane of the corpus callosum is shown in the upper right inset. The process is repeated for both the left and right hemispheres. Scale bar: 1 cm.

The estimated fiber bundles passing through seed points in the VOI of the left occipital lobe are shown in the left panel of FIGURE 1 for one representative child. The inset image shows a coronal view of the VOI. The subset of these fiber bundles that also pass through the corpus callosum are shown in the right panel of FIGURE 1. These comprise about 15% of the total left occipital lobe fiber bundles. The inset image shows the location within the splenium (the posterior callosum) of the fiber bundle estimates from the left hemisphere. Using these methods, DTI-FT identifies mainly callosal bundles projecting to the dorsal and medial cortical surface. We suspect that callosal tracts projecting to the lateral and ventral surfaces exist,[32,33] but they are missed by current methods.[7]

FIGURE 2 is a qualitative overview of the overlap between the right and left occipital-callosal fiber bundles in the individual brains. Each image section shows estimates from a different child. The images are cropped to show the posterior portion of the corpus callosum, including the splenium and the isthmus.

In these children, just as in adults, the left and right occipital-callosal fiber positions overlap substantially in the splenium. Fiber bundles from the occipital lobe in the right that travel to, say, the temporal lobe in the left would not be part of this overlap. Hence, the high degree of overlap confirms the hypothesis that the majority of occipital lobe callosal fibers project to the contralateral occipital lobe.

FIGURE 2 also illustrates the significant size and shape variability of the splenium and isthmus. For example, consider the first image section. That child has a nearly circular splenium and a very narrow isthmus that is easy to identify. The last two subjects have a long, cylindrical splenium, and it is hard to identify the isthmus.

The traditional method of segmenting the callosum assigns a much larger splenial area to the last subject than the first. Yet, the estimated occipital-callosal fiber bundles are very similar in cross-sectional area. Hence, DTI-FT should provide a more secure method for segmenting the callosum into bands that correspond to functional units compared to conventional segmentation definitions based on callosal shape.[34]

The agreement between subjects in the shape and position of the occipital-callosal fiber bundles at the midsagittal plane encouraged us to pool the data into a single image. We did this in two ways. First, we transformed the individual subject data into a common spatial reference frame based on the position of the anterior and posterior commissures (see METHODS). To quantify the left–right convergence, we defined a grid comprising 0.5×0.5 mm bins. The grid was placed at a position that was 36 mm posterior to the AC and 11 mm above the AC–PC line in the midsagittal plane. For each bin, we calculated the fiber bundle density estimates (bundles per square mm per subject) from the left and right occipital lobes. The correlation between these two values is shown in a scatter plot (FIG. 3A). These estimates obtained from the left and right data sets are highly correlated, with a linear regression accounting for 86% of the variance. Within each bin, we estimated on average 10% more fiber bundles arriving from the left occipital lobe. The spatial distributions within the splenium of the left and right fiber bundle density estimates are shown in the images of FIGURE 3B.

As noted above, across individuals there is considerable variation in the shape and position of the splenium with respect to the AC. For example, in this co-registered coordinate frame, it is still possible for the center of the splenium between two subjects to differ by a centimeter. To improve the coarse alignment based on the AC and PC positions, we placed the center of mass of each subject's occipital-

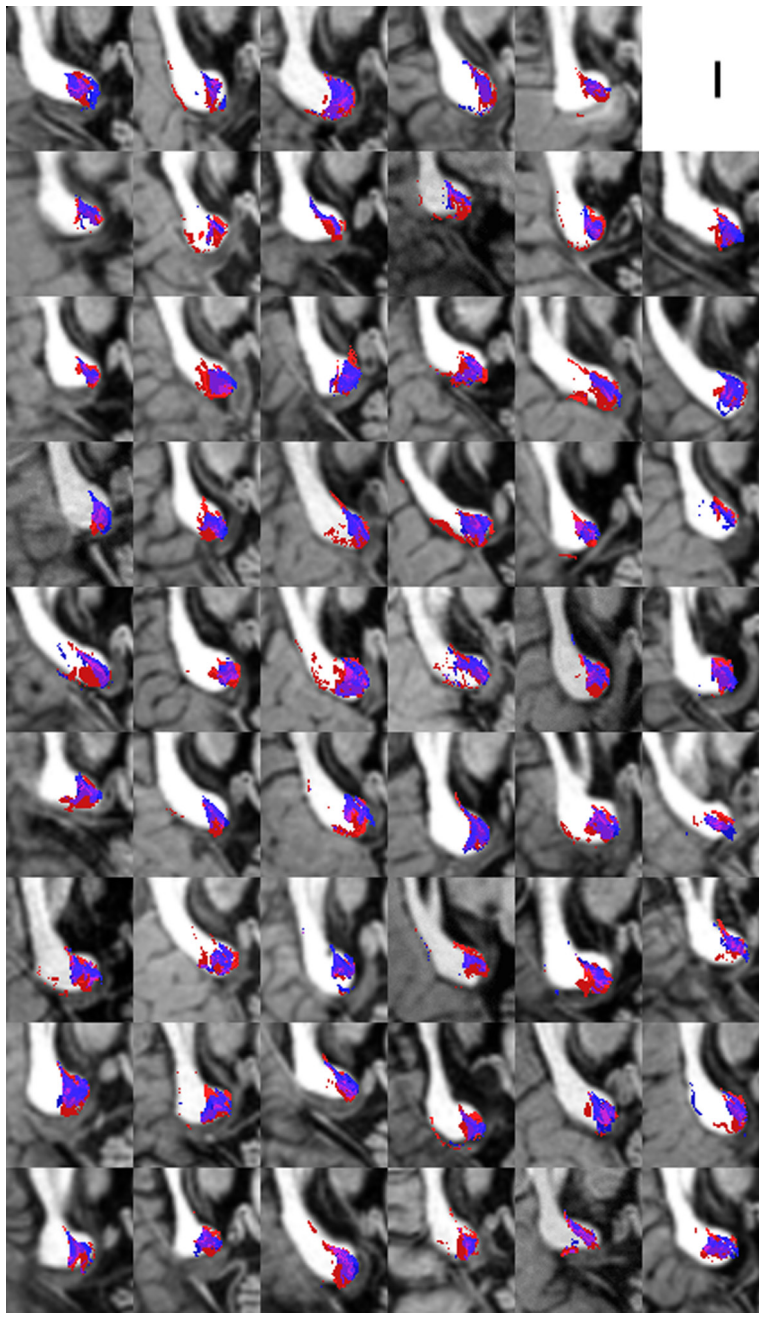

FIGURE 2. Left and right occipital-callosal fiber bundle positions in 53 children. The positions of fiber bundles estimated from left (red) and right (blue) occipital lobes are indicated by the color overlay. A pixel is colored if there is at least one estimated fiber bundle at that location. Scale bar: 1 cm.

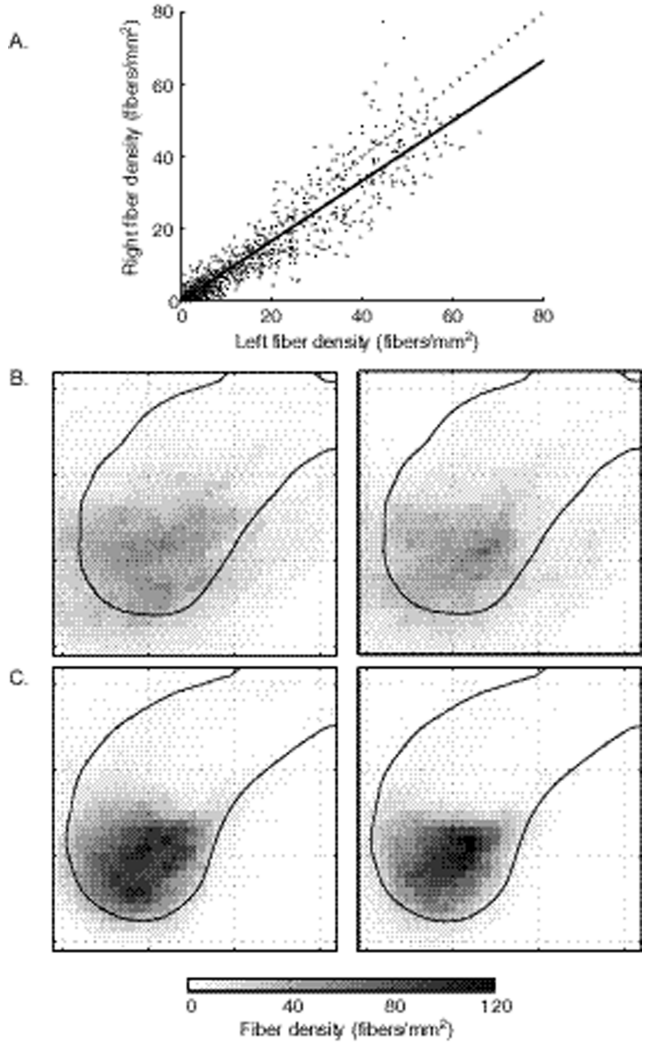

FIGURE 3. Convergence of occipital-callosal fiber bundle densities estimated independently in the left and right hemispheres. The data are cumulated from all 53 children. **(A)** The data from each child were translated and scaled into a common coordinate frame, aligned with the AC–PC axis. The graph compares the number of fiber bundles per square mm (per subject) from the left (horizontal axis) and right (vertical axis) at locations within a grid drawn in the corpus callosum. **(B)** The images show the fiber bundle density estimates overlaid on a contour that represents the average splenium in AC–PC aligned coordinates. These data form the basis of the graph in panel A. The two images show the spatial distribution of the fibers derived from the left (*left panel*) and right (*right panel*) occipital lobes. **(C)** The data from each child were translated in two dimensions so that the combined center of mass of left and right occipital-callosal fiber bundles is at a common location. This translation reduces the variance caused by errors in registering the brains. Grid lines are spaced at 5 mm.

callosal fiber bundles at a common position. The images in FIGURE 3C show the fiber bundle density estimates overlaid after aligning each subject in this way. Again, the right and left fiber density bundle estimates agree quite closely (the percent variance explained increases to 94%). The shape of the occipital-callosal fiber bundles is more apparent, and with this alignment it becomes clear that the fiber bundles pass mainly through the most ventral portion of the splenium.

The occipital-callosal fibers can be further subdivided according to their cortical projection zones. We defined three regions of interest (ROIs) corresponding to the anatomical positions of several visual field maps on the cortical surface of one

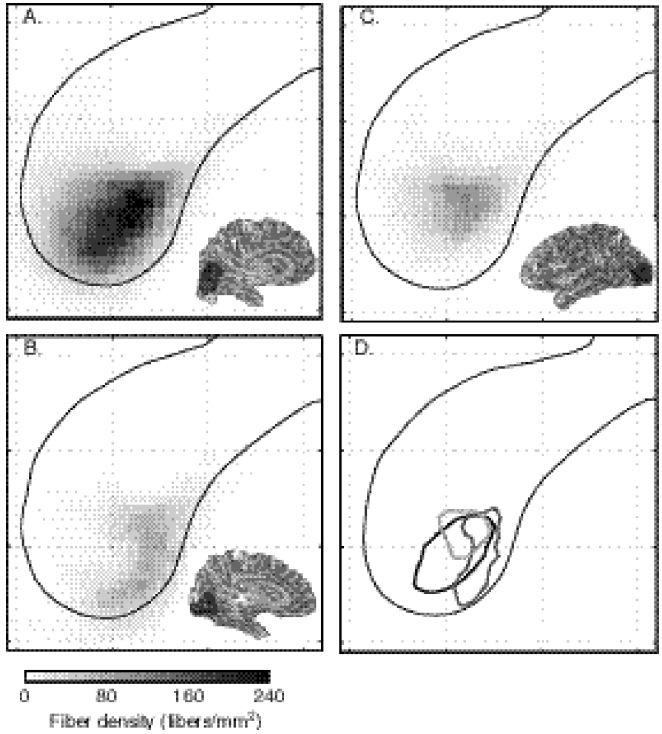

FIGURE 4. Segmentation of the occipital-callosal fiber bundles according to cortical projection zone. The four panels show the distribution of the fibers that terminate near three distinct occipital projection zones. The inset figures show a smoothed version of the cortex at the boundary between white and gray matter. The shading describes the gyri (light) and sulci (dark). The cortical region of interest is shown by the dark overlay. **(A)** The largest group of estimated fibers terminate in the dorsal region of the occipital cortex. **(B)** Fibers located in the anterior-ventral splenium terminate near the ventral occipital surface. **(C)** Fibers terminating in the posterior and lateral aspect of the occipital lobe, which include mainly foveal representations, form a small localized group near the middle of the spenium. **(D)** The contour lines that capture 60% of the fibers within each group are shown with respect to the outline of the splenium (dorsal is black, ventral is dark gray, and lateral is light gray). Grid lines are spaced at 5 mm.

representative subject. The ROIs were warped to the native space of each individual subject by first warping them to the standard space of our template brain and then warping them to each individual brain (using the reverse of the template deformation). The first region is dorsal to the fundus of the calcarine sulcus and roughly corresponds to the dorsal portions of V1, V2, V3, V3A, and V3B maps. A second ROI was defined ventral to calcarine and includes the ventral portions of V1, V2, V3, and all of hV4. Finally, a third ROI was defined on the cortical surface covering the occipital pole and extending onto the lateral surface into the lateral-occipital complex.[35,36] We confirmed that these warped ROIs were anatomically reasonable in each of the individual brains (e.g., the dorsal/ventral split fell within the calcarine sulcus).

We subdivided the center of mass–aligned occipital-callosal fiber bundles based on the cortical ROIs closest to each fiber bundle end point (see ref. 7 for details). The fiber bundle density plots for the three ROIs are shown in FIGURES 4A, 4B, and 4C. The largest percentage of the occipital-callosal fiber bundles project to dorsal cortex; the fiber bundles projecting to ventral cortex are slightly anterior and ventral. The lateral-occipital projecting fibers overlap the other two groups in the superior-anterior region. Damage near this position can produce alexia.[17] The contours in FIGURE 4D outline the regions containing 60% of the estimated fiber densities from each of the subgroups.

We computed an atlas to summarize the regularities across the entire group of children. This atlas includes the diffusion tensor data from all 53 children; it was created by finding smooth deformations of each individual brain via a common reference frame (see METHODS). The atlas data from a single axial slice through the splenium are shown in FIGURE 5. The atlas includes both fractional anisotropy (FA) and principal diffusion direction (PDD) measures.

Mean and standard deviation of the measured FA are overlaid on the average anatomical image (FIGS. 5A and 5B). Only locations with a mean FA value above 0.2 are shown in the overlay. The FA values are very high in the callosal pathways (~0.6–0.8) and in general in the dense medial white matter regions of the brain. The typical FA value decreases steadily as the measurements approach the cortical surface. Also, note that the FA standard deviation tends to be lowest at the center of a major pathway, increasing towards the edge. This tendency can be explained by imperfections in the alignment of the multiple brains. Small misalignments in the middle of a major white matter tract do not introduce significant FA variation, while misalignments at the edge where FA contrast is high will produce significant variance in the atlas.

The FA standard deviation is also very high in the splenium and forceps major; the standard deviation is particularly high where the forceps major passes adjacent to the lateral horn of the occipital ventricle. The standard deviation in this region is approximately that of a uniform distribution on the unit interval (0.2887). Hence, atlas-based methods are insensitive for identifying FA group differences in this region.

The PDD mean and dispersion in the same slice are shown in FIGURES 5C and 5D. The dispersion is measured using the bipolar Watson distribution, which describes an antipodal symmetric distribution of unsigned random vectors on a unit sphere.[37] The mean direction is quite stable within the internal capsule and corpus callosum. Approaching the edges of the white matter (e.g., in the posterior occipital lobe), the PDD becomes very variable. In this case, the maximum dispersion for a uniformly distributed set of directions is 55°. Hence, the PDD at this slice in the posterior occipital lobe is almost randomly distributed.

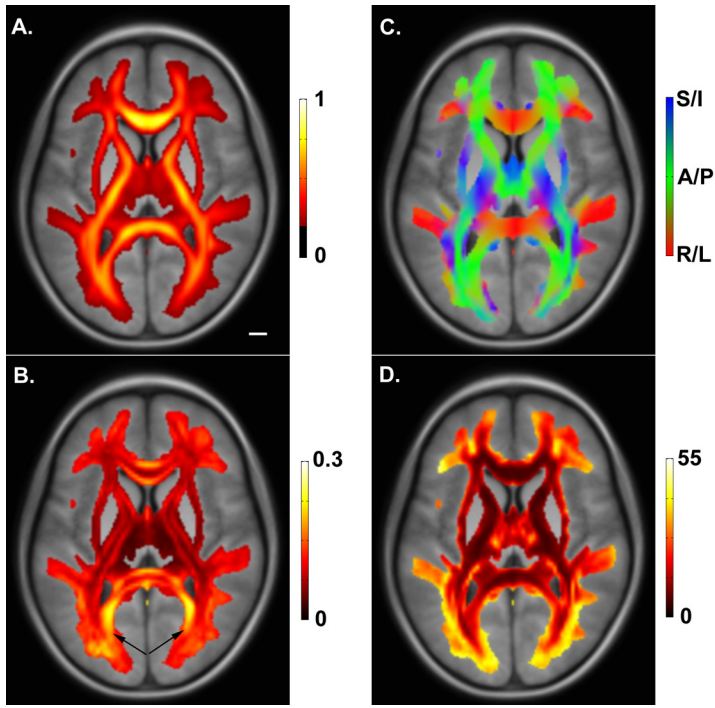

FIGURE 5. A single slice from the atlas summarizing the children's DTI measurements. The DTI information is superimposed on the mean anatomical image from coregistering the 53 brains. **(A)** The color overlay represents the mean fractional anisotropy (FA). **(B)** The standard deviation of the FA. **(C)** The principal diffusion direction (PDD): S/I, superior/inferior; A/P, anterior/posterior; R/L, right/left. **(D)** The PDD reliability is represented by the angular dispersion (in degrees). This statistic represents the angular scatter of the PDD on the unit sphere. Scale bar: 1 cm.

These images clarify that atlas-based methods have much higher sensitivity (lower variance) in some brain regions than others. The group data have relatively low variance near the sagittal midline, but the reliability of both PDD and FA maps declines severely near the cortical surface. This uneven sensitivity pattern should be part of the interpretation of any DTI result. For example, two recent studies demonstrated a covariation of reading performance with FA in a portion of the atlas with very low FA variance.[13,14] The atlas images remind us that such covariation between DTI data and behavior may be present elsewhere, but missed because of high group variance in those regions.

There is good agreement in the estimates of occipital-callosal fibers tracked independently from the two hemispheres in individual subjects (FIGS. 2 and 3). Considering the atlas data, we find that it should be possible to track reliably fiber bundle paths that course through the corpus callosum and pass near the ventricles. This is because the reliability of the PDD in this portion of the brain is relatively high; while the FA reliability is low in some of these regions, the mean FA value is high enough

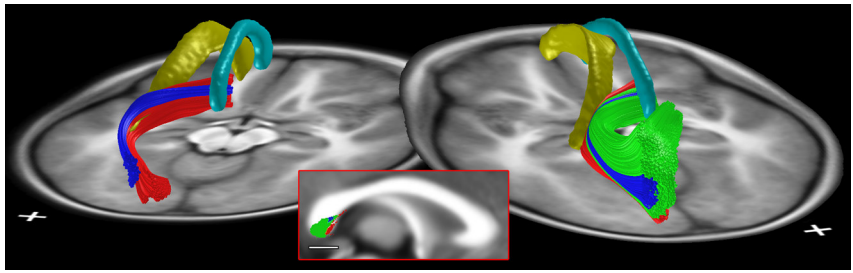

FIGURE 6. Fiber bundle pathways between the callosum and three regions of interest on the cortical surface. The fiber bundles are derived from the average tensor maps. The image on the left shows the pathways followed by the fibers that terminate near the ventral (red) and lateral occipital (blue) cortical regions of interest (see FIG. 4). The ventral fibers pass on both sides of the lateral ventricle (shown in dark yellow), forming part of the tapetum. The image on the right shows these same fibers from a different viewpoint and adds the largest group of fibers, those that terminate near the dorsal region of interest (green). The inset image shows the location of these fiber groups within the splenium. The corpus callosum is shown in cyan. Scale bar: 1 cm.

to support estimation of the mean PDD. We estimated the path followed by the occipital-callosal bundles that connect the callosum and the three cortically defined ROIs (FIG. 6). The lateral occipital fiber bundles follow a path that is mainly superior to the lateral occipital ventricle. The fibers headed towards the ventral occipital lobe divide, with some fibers passing superior and others inferior to the ventricle. The division of these fibers around the ventricle is present in the atlas, and it also can be seen in many individual subjects. The spatial relationship between these fiber bundles, the lateral occipital ventricle, and the callosum are illustrated by the image on the left. The dorsal fiber bundles are the largest group. These are added in to the image on the right. The positions of these different fiber bundles within the splenium are shown by the inset image.

DISCUSSION

The occipital-callosal fiber bundles estimated in children are quite similar to previous estimates from a much smaller adult data set. In both cases, the independent estimates from right and left hemisphere data converge into a small region within the splenium of the corpus callosum. Further, the data from the larger sample of children can be used to quantify the precision of the estimates. Positions of the occipital-callosal fiber bundles within the splenium appear to be accurate to within 1 mm in individual subjects (FIGS. 2–4).

DTI, like any measurement modality, has strengths and limitations. The measurements of these occipital-callosal fibers are reliable and can be made at very high spatial resolution. On the other hand, we find very limited ability to identify fiber bundles that pass through the corpus callosum to the lateral surface. These pathways interdigitate through much larger pathways that form the inferior longitudinal fasciculus (occipitofrontal and occipitotemporal pathways[4]). The current data and analysis methods cannot resolve the smaller pathways in this region of fiber crossing.

DTI Sensitivity in Group Analyses

In some cases, it is essential to analyze data from individual subjects, say for diagnosis and treatment. The measurements described here confirm the validity of the DTI-FT methods for identifying such pathways in certain parts of the brain. In other cases, it can be useful to pool data across subjects into an atlas, which represents the expected pattern in the "average" brain for a given population. The atlas identifies common points and permits testing of various statistical hypotheses, such as a covariation between reading skill and white matter anisotropy.[13,14,38]

While atlases can increase statistical power, they also have significant limitations. Some of these limitations are made explicit by including both mean and variance values in the atlas (FIG. 5). The group atlas for DTI shows that the reliability of FA and PDD values is inhomogeneous across the brain. In general, measurements from the internal capsule and inferior longitudinal fasciculus are quite reliable; group averages in other regions, such as near the lateral occipital or frontal regions, are much less so. Consequently, smaller differences can be detected in some regions compared to others. This may be a factor in explaining the tendency to find significant covariation with other factors in a small number of low variance regions (e.g., ref. 39).

The reliability of the atlas data also has implications for the ability to track fiber bundles from group data (e.g., ref. 9). A fiber bundle may be reliably detected in each individual, but coregistration of many individuals may introduce FA and PDD variance that masks the bundle in the average. Moreover, if there is a systematic bias in the individual data, such as fibers taking a wrong turn into a major bundle of crossing fibers, this bias will not be eliminated (and may be accentuated) in the group average. It is essential to be alert to these uncertainties and limitations when interpreting DTI-FT in group data. In general, if care is taken to ensure that the major pathways are present in the group average data, then fiber bundles identified in the atlas are a convenient way to summarize expected pathway positions in a "typical" brain (FIG. 6).

Splenial Pathways Necessary for Reading

More than a hundred years of neurology has focused attention on the loss of reading (alexia) following white matter damage in the splenium and nearby occipital and temporal pathways.[1,40] Careful neurological analyses show that alexia is closely coupled to damage in the splenium, forceps major, and white matter above the occipital horn.[17,19] On the other hand, the fibers passing ventromedial to the occipital ventricle are "of little importance for reading" (p. 1822 of ref. 19). Concerning the location of these fibers in the splenium, it appears that "only one group … seems to be pertinent for reading. That corresponds roughly to the middle component of fibers of the splenium, considered on the dorso-ventral axis …" (p. 1580 of ref. 17).

Thus, the region of the splenium containing fiber bundles essential for reading likely includes the fibers we have identified that form the superior and lateral wall of the lateral ventricle (FIG. 6). These bundles also pass through the central part of the dorsal-ventral axis in the splenium. The fibers in the splenium that are slightly superior to the ones we have identified connect with the lateral temporal and medial parietal pathways.[34] The parietal fibers can be identified, and with additional work it may be possible to follow the fibers that pass to the lateral aspect of the temporal lobe. The identification of these splenial pathways builds upon the classic neuro-

logical findings and, when coupled with functional measurements, may contribute to a better understanding of the reading pathways in normal developing children.

ACKNOWLEDGMENTS

We thank Jan Ruby, Adele Behn, and Sweta Patanaik for their work recruiting subjects and organizing the data. We also gratefully acknowledge the cheerful and helpful cooperation of the parents and children who participated in this study. Funding was provided by NIH Grant No. EY015000 and the Schwab Foundation for Learning.

REFERENCES

1. DEJERINE, J. 1891. Sur un cas de cecite verbale avec agraphie, suivi d'autopsie. Mém. Soc. Biol. **3:** 197–201.
2. JUST, M.A. *et al*. 2004. Cortical activation and synchronization during sentence comprehension in high-functioning autism: evidence of underconnectivity. Brain **127:** 1811–1821.
3. BASSER, P.J. *et al*. 2000. *In vivo* fiber tractography using DT-MRI data. Magn. Reson. Med. **44:** 625–632.
4. CATANI, M. *et al*. 2002. Virtual *in vivo* interactive dissection of white matter fasciculi in the human brain. Neuroimage **17:** 77–94.
5. CATANI, M. *et al*. 2003. Occipito-temporal connections in the human brain. Brain **126:** 2093–2107.
6. CONTURO, T.E. *et al*. 1999. Tracking neuronal fiber pathways in the living human brain. Proc. Natl. Acad. Sci. USA **96:** 10422–10427.
7. DOUGHERTY, R.F. *et al*. 2005. Functional organization of human occipital-callosal fiber tracts. Proc. Natl. Acad. Sci. USA **102:** 7350–7355.
8. HAGMANN, P. *et al*. 2003. DTI mapping of human brain connectivity: statistical fibre tracking and virtual dissection. Neuroimage **19:** 545–554.
9. JONES, D.K. *et al*. 2002. Spatial normalization and averaging of diffusion tensor MRI data sets. Neuroimage **17:** 592–617.
10. MORI, S. *et al*. 1999. Three-dimensional tracking of axonal projections in the brain by magnetic resonance imaging. Ann. Neurol. **45:** 265–269.
11. MORI, S. *et al*. 2002. Imaging cortical association tracts in the human brain using diffusion-tensor-based axonal tracking. Magn. Reson. Med. **47:** 215–223.
12. MOSELEY, M., R. BAMMER & J. ILLES. 2002. Diffusion-tensor imaging of cognitive performance. Brain Cogn. **50:** 396–413.
13. KLINGBERG, T. *et al*. 2000. Microstructure of temporo-parietal white matter as a basis for reading ability: evidence from diffusion tensor magnetic resonance imaging. Neuron **25:** 493–500.
14. DEUTSCH, G.K. *et al*. 2005. Children's reading performance is correlated with white matter structure measured by diffusion tensor imaging. Cortex **41:** 354–363.
15. MOLKO, N. *et al*. 2002. Visualizing the neural bases of a disconnection syndrome with diffusion tensor imaging. J. Cogn. Neurosci. **14:** 629–636.
16. WAKANA, S. *et al*. 2004. Fiber tract-based atlas of human white matter anatomy. Radiology **230:** 77–87.
17. DAMASIO, A.R. & H. DAMASIO. 1983. The anatomic basis of pure alexia. Neurology **33:** 1573–1583.
18. LE, T.H. *et al*. 2005. Diffusion tensor imaging with three-dimensional fiber tractography of traumatic axonal shearing injury: an imaging correlate for the posterior callosal "disconnection" syndrome—case report. Neurosurgery **56:** 189.
19. BINDER, J.R. & J.P. MOHR. 1992. The topography of callosal reading pathways: a case-control analysis. Brain **115**(part 6)**:** 1807–1826.

20. MAO-DRAAYER, Y. & H. PANITCH. 2004. Alexia without agraphia in multiple sclerosis: case report with magnetic resonance imaging localization. Mult. Scler. **10:** 705–707.
21. BAMMER, R. & M. AUER. 2001. Correction of eddy-current induced image warping in diffusion-weighted single-shot EPI using constrained non-rigid mutual information image registration. *In* Proceedings of the Ninth Annual ISMRM Meeting. Vol. 9, p. 508.
22. BASSER, P.J. 1995. Inferring microstructural features and the physiological state of tissues from diffusion-weighted images. NMR Biomed. **8:** 333–344.
23. BASSER, P.J. & C. PIERPAOLI. 1996. Microstructural and physiological features of tissues elucidated by quantitative-diffusion-tensor MRI. J. Magn. Reson. **B111:** 209–219.
24. HEDEHUS, M. & S. SKARE. 2004. DTI post-processing using "tensorcalc" software.
25. FRISTON, K., J. ASHBURNER & WELLCOME DEPARTMENT OF IMAGING NEUROSCIENCE. 2004. Statistical parametric mapping.
26. PAJEVIC, S., A. ALDROUBI & P.J. BASSER. 2002. A continuous tensor field approximation of discrete DT-MRI data for extracting microstructural and architectural features of tissue. J. Magn. Reson. **154:** 85–100.
27. ALEXANDER, D.C. *et al*. 2001. Spatial transformations of diffusion tensor magnetic resonance images. IEEE Trans. Med. Imaging. **20:** 1131–1139.
28. PRESS, W.H. *et al*. 2002. Numerical Recipes in C++: The Art of Scientific Computing. Cambridge University Press. London/New York.
29. SMITH, S.M. 2002. Fast robust automated brain extraction. Hum. Brain Map. **17:** 143–155.
30. ASHBURNER, J. & K.J. FRISTON. 1999. Nonlinear spatial normalization using basis functions. Hum. Brain Map. **7:** 254–266.
31. ALEXANDER, A.L. *et al*. 2000. A geometric analysis of diffusion tensor measurements of the human brain. Magn. Reson. Med. **44:** 283–291.
32. KRIEG, W.J.S. 1963. Connections of the Cerebral Cortex. Brain Books. Evanston, IL.
33. CLARKE, S. & J. MIKLOSSY. 1990. Occipital cortex in man: organization of callosal connections, related myelo- and cytoarchitecture, and putative boundaries of functional visual areas. J. Comp. Neurol. **298:** 188–214.
34. HUANG, H. *et al*. 2005. DTI tractography based parcellation of white matter: application to the mid-sagittal morphology of corpus callosum. Neuroimage **26:** 195–205.
35. WANDELL, B.A., A.A. BREWER & R.F. DOUGHERTY. 2005. Visual field map clusters in human cortex. Philos. Trans. R. Soc. Lond. B Biol. Sci. **360:** 693–707.
36. GRILL-SPECTOR, K. & R. MALACH. 2004. The human visual cortex. Annu. Rev. Neurosci. **27:** 649–677.
37. SCHWARTZMAN, A., R.F. DOUGHERTY & J.E. TAYLOR. 2005. Cross-subject comparison of principal diffusion direction maps. Magn. Reson. Med. **53:** 1423–1431.
38. BEAULIEU, C. *et al*. 2005. Imaging brain connectivity in children with diverse reading ability. Neuroimage **25:** 1266–1271.
39. SALAT, D.H. *et al*. 2005. Age-related alterations in white matter microstructure measured by diffusion tensor imaging. Neurobiol. Aging **26:** 1215–1227.
40. DEJERINE, J. 1892. Contribution a l'étude anatomoclinique et clinique des differentes varietes de cecite verbal. C. R. Hebd. Séances Mém. Soc. Biol. **4:** 61–90.